

Observational evidence from direct current measurements for propagation of remotely forced waves on the shelf off the west coast of India

P. Amol¹, D. Shankar¹, S. G. Aparna¹, S. S. C. Shenoi², V. Fernando¹, S. R. Shetye¹, A. Mukherjee¹,
Y. Agarvadekar¹, S. Khalap¹, and N. P. Satelkar¹

¹ National Institute of Oceanography, Dona Paula, Goa, India, 403004

² INCOIS, Ocean Valley, Pragathi Nagar (BO), Nizampet (SO), Hyderabad, 500090

Abstract

We use data from six Acoustic Doppler Current Profiler (ADCP) moorings deployed during March–September 2008 on the continental shelf and slope off Bhatkal, Goa, and Jaigarh on the central west coast of India to present evidence for poleward propagation of shelf or coastal-trapped waves (CTWs). Wave propagation is seen on the shelf in the 20–40-day, 10–14-day, and 3–5-day-period bands. The lag from south to north indicates that remote forcing is important even at periods as short as 4 days. Using QuikSCAT wind data, we show that the contribution of remote forcing to the shelf West Indian Coastal Current (WICC) is significant even when the local alongshore wind is strong, as during the summer-monsoon onset during May–June, and forces a strong local response that masks the effect of remote forcing. Forced wave calculations using CTW theory show that remote forcing of the WICC is present at all times, but is most striking when the local winds are weak, as during March–April. The CTW calculations show that the source region for the remote forcing may extend beyond the west coast into the Gulf of Mannar between India and Sri Lanka. On the slope, propagation is seen only at the 4-day period. At higher periods, the slope WICC decorrelates rapidly along the coast, but upward phase propagation, implying downward propagation of energy associated with poleward propagation, is evident even at these higher periods.

1 Introduction

Just as the circulation in the North Indian Ocean (NIO) (Figure 1b) reverses seasonally in response to the reversing monsoon winds (see, for example, the atlas of *Wyrtki* [1971], or the review of *Schott and McCreary* [2001]), so does the current off the Indian west coast (see, for example, the review by *Shetye and Gouveia* [1998]), which has been called the West India Coastal Current (WICC) [*Shankar and Shetye*, 1997]. Most of our earlier knowledge of the WICC was based on hydrographic data

[*Shetye et al.*, 1990, 1991, *Stramma et al.*, 1996], ship drifts [*Shetye et al.*, 1994], and surface drifters [*Shenoi et al.*, 1999], which could describe, at best, the seasonal cycle of the current. The advent of satellite altimetry presented a more comprehensive basin-wide view of the circulation and led to the discovery of the Lakshadweep High and Low in the southeastern Arabian Sea (SEAS) [*Bruce et al.*, 1994, *Shankar and Shetye*, 1997]; the high and low in sea level, once identified in altimeter data, were apparent in earlier hydrographic data too [*Bruce et al.*, 1994]. A monthly climatology of the WICC based on ship drifts [*Mariano et al.*, 1995] and a weekly climatology of its geostrophic component based on altimeter sea-level anomalies (SLAs) show a distinct seasonal cycle of the WICC (Figure 1c,d). The WICC flows equatorward during the Indian summer monsoon (May–September) and poleward during the winter monsoon (November–February). Below the surface current, the hydrographic data suggested the presence of an undercurrent [*Shetye et al.*, 1990, 1991].

Direct current measurements have been few in the region and have been restricted to short durations, typically a month or less; these short-duration data enabled the description of the major tidal constituents and high-frequency (period of the order of a few days) wind-driven currents [*Varkey*, 1980, *Shenoi et al.*, 1998, *Unnikrishnan and Antony*, 1990, *Shenoi and Antony*, 1991, *Antony and Shenoi*, 1993, *Kumar and Kumar*, 1996, *Kumar and Srinivas*, 2007, *Shetye et al.*, 2008], but the latter were restricted to a few isolated measurements.

Given this paucity of data that can resolve the variability at time scales other than the seasonal, it is not surprising that most of the theoretical studies of the WICC have been restricted to explaining the seasonal cycle [*McCreary et al.*, 1993, *Bruce et al.*, 1994, *Shankar and Shetye*, 1997, *Shankar et al.*, 2002] and the heat budget [*Durand et al.*, 2004] of and salinity variation [*Durand et al.*, 2007, *Kurian and Vinayachandran*, 2007] in the SEAS at seasonal time scales. These studies showed that the seasonal cycle of the WICC is intimately linked to the wind-driven basin-scale dynamics of the NIO. Of particular interest are the following results. First, the seasonal cycle of the WICC is explicable by linear wave theory [*Shankar and Shetye*, 1997]. Second, this seasonal cycle is driven more by winds that blow along the east coast of India than by the local, west-coast winds [*McCreary et al.*, 1993, *Shankar and Shetye*, 1997, *Shankar et al.*, 2002]. One reason for this stronger effect of remote forcing from the Indian east coast, compared to the effect of forcing by the local, west-coast winds, on the WICC is that the local winds have a much weaker alongshore component than do the winds along the Indian east coast because the axis of the seasonal wind field is largely normal (parallel) to the west (east) coast [*Shankar et al.*, 2002]. The stronger alongshore winds off

the Indian east coast force coastal Kelvin waves that propagate equatorward along the coast and turn around Sri Lanka to propagate poleward along the west coast. In the process of propagating poleward along this eastern-ocean boundary, they radiate westward-propagating Rossby waves. Third, these modelling studies show that dynamics merges the Arabian Sea, the Bay of Bengal, and the Equatorial Indian Ocean (EIO) into a single entity, making it essential to model the entire Indian Ocean to simulate the circulation in even a part like the west coast of India. Binding together the circulation in these sub-basins of the Indian Ocean are three long, baroclinic waves: the Equatorial Kelvin and Rossby waves and coastal Kelvin waves. Along the west coast, the coastal Kelvin waves propagate from south to north at the sub-inertial frequencies of interest.

At intraseasonal time scales, however, the paucity of data has implied a dearth of similar theoretical studies for the Indian coastal currents; such studies of intraseasonal variability are largely restricted to the EIO because time-series data on currents are available in that region [*Sengupta et al.*, 2004, *Miyama et al.*, 2006, *Ogata et al.*, 2008] from moorings equipped with Acoustic Doppler Current Profilers (ADCPs). In order to map the variability of the currents along the Indian coast over a range of time scales, but in particular the variability at time scales shorter than a season, a set of ADCP moorings have been deployed off the coast of India in the last few years. The first description of the currents measured by these ADCPs was by *Vialard et al.* [2009], who showed that the intraseasonal variability of the WICC on the continental slope off Goa (see Figure 1a for location) over a two-year period during 2006–2008 was much stronger than the seasonal cycle, which was very weak. In contrast, the altimeter SLAs showed comparable seasonal and intraseasonal variability. This difference between the SLAs and current was ascribed to the radiation of Rossby waves from the coast. Since the westward-propagating Rossby waves do not exist at intraseasonal periods for the gravest baroclinic mode at the latitude of the Goa ADCP mooring, the intraseasonal SLAs did not propagate offshore and this trapping led to the stronger intraseasonal WICC component. At seasonal time scales, the Rossby waves exist almost throughout the NIO, and the offshore propagation weakens the cross-shore sea-level gradient and therefore the seasonal WICC off Goa.

All these studies, including that of *Vialard et al.* [2009], have been restricted to the continental slope and the deeper ocean owing to the paucity of data from the shelf regime. Direct current measurements on the shelf have been restricted to the short current-meter records mentioned above. On such set of one-month-long current-meter measurements made during March–April 2003 in the near-coastal shelf regime (water-column depth 10–20 m) off Goa were used by *Shetye et al.* [2008] to show that the observed current could not be forced by the local wind alone. At periods less

than 10 days, the local wind and current were highly correlated, leading *Shetye et al.* [2008] to infer dominance of local forcing at these periods. At periods greater than 10 days, the local wind was unidirectional, but the currents reversed during the month; the source of this current reversal was traced over 600 km south of the current meters to Kollam on the southwest coast of India (Figure 1a), leading them to infer the existence of remote forcing by shelf waves. Like the Kelvin wave, for which the shelf break is assumed to be a vertical wall, at the sub-inertial periods of interest, these shelf waves propagate with the coast on their right in the northern hemisphere. Nevertheless, even this data record, like other current-meter records in the region, was too short to map the range of intraseasonal frequencies expected to be seen in the WICC.

Similar propagating waves have been noted on the continental shelf elsewhere too. Eastern-boundary examples include the west coast of the United States [*Wang and Mooers*, 1976, *Clarke*, 1977, *Hickey*, 1984, *Hickey et al.*, 2003, *Martinez and Allen*, 2004] and the west coast of South America [*Smith*, 1984, *Brink*, 1982b], while western-boundary examples include the Grand Banks, where local winds were found to drive currents in the inner shelf, with the wind-current correlation decreasing offshore [*DeTracey et al.*, 1996], and the Labrador shelf, where the local winds forced just 30% of the observed bottom-pressure variability [*Middleton and Wright*, 1991]. Shelf waves have also been observed and modelled off the coast of Australia [*Hamon*, 1966, *Middleton and Cunningham*, 1984, *Freeland et al.*, 1986, *Church et al.*, 1986, *Clarke*, 1987]. The comprehensive work done in the 1960s and 1970s on the shelf waves are summarized by *Mysak* [1980]. Later studies assembled a body of theory for arbitrary shelf topography and showed that it is possible to separate the local and remote forcing using Coastal-Trapped-Wave (CTW) models [*Brink*, 1982a,b, *Battisti and Hickey*, 1984, *Mitchum and Clarke*, 1986, *Wilkin and Chapman*, 1987, *Clarke and Gorder*, 1986, *Lopez and Clarke*, 1989, *Hickey et al.*, 1991]. More recently, *Maiwa et al.* [2010] used a general-circulation model to study CTWs off the southern and eastern coasts of Australia.

In this paper, we present data from a set of three mooring pairs located roughly 200 km apart on the shelf and slope off the central west coast of India; the Goa moorings form the central pair in this three-pair set, and the data presented by *Vialard et al.* [2009] was from the slope mooring. We use these data to show the following. First, we present direct evidence for propagation of waves on the shelf. Second, propagating waves exist even at periods as short as four days. Third, there are times when this propagation is masked by strong local forcing. Fourth, CTW theory is used to trace the source region of the remote forcing. Fifth, there is a difference between the WICC variability observed on the shelf and slope, with propagating waves not as evident on the slope for

periods above four days.

We begin by describing the data sources in Section 2. The raw currents on both shelf and slope are presented in Section 3, followed in Section 4 by an analysis showing evidence for propagating waves on the shelf. CTW theory is used in Section 5 to separate local and remote forcing on the shelf. Section 6 concludes the paper.

2 Data, processing, and analysis

Six upward-looking RDI ADCPs were deployed for about six months during March-October 2008 (see Table 1 for details) along the central west coast of India; the moorings were located in pairs approximately at 13.6°N (off Bhatkal), 15.1°N (off Goa), and 17.1°N (off Jaigarh) (Figure 1a). Each pair consisted of a mooring on the continental shelf (slope) at a water-column depth of about 100 m (1000 m). The moorings were separated by 150–200 km along the coast and about 50 km across the shelf-break. The shelf ADCPs (300 kHz) were located just above the bottom with a sampling interval of 15 minutes, but the slope ADCPs (75 kHz) were located about 350–400 m below the surface with a sampling interval of one hour. Off Goa, the slope ADCP was deployed at a depth of about 170 m. The accuracy of the velocity measurements was better than 1.55 cm s^{-1} .

The currents were detided using the Tidal Analysis Software Kit (TASK) [Bell *et al.*, 1998] with a one-month control file, which removes all the dominant tidal components with period less than one month. Since the dominant wind-driven flow is alongshore, the detided currents were rotated to estimate the alongshore and cross-shore components by minimizing the latter using least squares. The angle of rotation is given in Table 1. Only alongshore components of the currents are analysed here. The inertial period at the southernmost mooring (Bhatkal) is 2.1 days. Since our interest is in variability at periods greater than the inertial period, we applied a 2.5-day low-pass, fourth-order Butterworth filter to all the current data.

Daily wind data were obtained from the QuikSCAT scatterometer. An earlier study [Aparna *et al.*, 2005] has shown that the QuikSCAT wind vector correlates well with the wind measured using an anemometer on the Indian west coast. Gridded data at a resolution of 0.5 were downloaded from <http://www.ifremer.fr/cersat/en/data/download/download.htm>. The winds were rotated using the average angle of the coast based on the QuikSCAT grid.

3 Alongshore currents

The alongshore currents (Figure 2) showed variation along the coast and across the shelf-break. The seasonal cycle described using hydrographic and ship-drift data was evident on the shelf off Goa and Jaigarh, where the current was largely equatorward during the summer monsoon, but was not as strong on the shelf off Bhatkal, where poleward intraseasonal bursts were seen during May–July. A poleward undercurrent was seen often off Goa, but not as often off Jaigarh; off Bhatkal, an equatorward undercurrent was seen during July and again in short bursts during August. The intraseasonal bursts were not evident simultaneously at all three locations, suggesting a lack of alongshore coherence in the intraseasonal variability. For example, the strong poleward bursts seen off Bhatkal during April and May–June were not seen off Goa, and much weaker poleward bursts were seen off Jaigarh during April–May. The current was strongest off Goa, where the peak speed was 55 cm s^{-1} ; it was distinctly weaker off Jaigarh.

On the slope, data were available for all ADCPs only in the depth range 55–170 m (Figure 2). In contrast to the shelf current, the slope current was strongest off Jaigarh and weakest off Goa. Except off Goa, where the current was largely equatorward during May–September, the seasonal cycle was not striking; the equatorward current off Bhatkal and Jaigarh was interrupted by several poleward bursts. At all locations, a poleward undercurrent was seen during May–September. These poleward sub-surface currents, located at a greater depth off Jaigarh (160–200 m) than off Bhatkal (130–150 m) (Figure 3), moved closer to the surface towards the end of the observations, suggesting upward phase propagation.

Empirical Orthogonal Function (EOF) analysis was used for an empirical decomposition of the currents into temporal and spatial modes; this decomposition was done separately for the shelf and slope, but for all three moorings along the coast, implying a restriction of the analysis to the depth and time range common to them. The first four modes accounted for over 90% of the variability on both shelf and slope, with the first two modes explaining over 75% of the variability (Figure 4).

On the shelf (Figure 4), all four modes were needed mainly to explain the variability at Bhatkal; the weaker current at Jaigarh had a much simpler vertical structure. Though EOFs do not pick specific frequencies for a given mode, the first mode, whose vertical structure was quasi-barotropic, was dominated by variability at a period of the order of a month during March–May, with higher frequencies also evident during the summer monsoon. The higher frequencies (period ranging from a few days to 10–15 days) were more prominent in the higher modes, whose vertical structure

accounted for the baroclinicity. The first two modes also suggested the presence of periods greater than 60 days, with the sign of the temporal vector for the second mode changing around the time of monsoon onset in June.

On the slope (Figure 4), the vertical structure was simplest off Goa, where the current did not reverse direction often over the top 180 m. In contrast to the shelf, the temporal vectors for the slope currents were dominated by a periodicity of the order of a month, with higher frequencies superimposed on them. These higher frequencies were more evident during the summer monsoon. The first and fourth mode also suggested the presence of periods greater than 60 days. An analysis was also done for the larger depth range common to the Bhatkal and Jaigarh moorings. A combination of the first two modes showed upward phase propagation, implying downward propagation of energy and propagation of waves along the slope.

EOF analysis, though useful because it picks empirically the variability common to all three moorings, has its limitations. It does not, for example, distinguish between low-frequency and high-frequency variability. An FFT (Fast Fourier Transform) analysis (not shown) showed common periodicities around 4 and 12 days for all moorings. The higher periods varied from 25–45 days, and a period around 7–8 days was also evident in a few moorings. The data (Figure 2) and the EOF analysis (Figure 4) showed a variation in the dominant frequencies over time, with higher frequencies more evident during the summer monsoon, but an FFT cannot account for such a temporal variation. Hence, we used the Morlet wavelet to perform a wavelet analysis of the currents. The analysis is presented for the 15 m (55 m) current on the shelf (slope) because our interest is primarily in the surface currents and these were the depth bins nearest the surface for which data were available for all moorings.

On the shelf, the wavelet transform at 15 m (Figure 5d–f) showed several distinct periodicities at different times. One prominent periodicity was about 32 days and occurred during March–May and August–September off Jaigarh and Goa. Off Bhatkal, two distinct bands, 16–27 days and 32–42 days, were seen during March–August and March–July, respectively. Wavelet power at a period around 12 days was also seen at all three locations, but it was strongest off Goa. The 4–day period, though weaker in comparison, was also evident at all three locations. Similar variability was seen at other depths.

At 55 m on the slope (Figure 5a–c), only the 32-day periodicity was common to all three locations. The variability in this period band was stronger during March–June for Bhatkal and May–July for Goa and Jaigarh. The 12–day band was also seen at all locations, but at different

times. Wavelet power was much less at periods less than 8 days, but variability was seen even at periods as low as 4 days at all locations. Similar variability was seen at other depths.

Since the highest of the intraseasonal periodicities seen on the slope was in the 30–48 day band, a useful separation between the intraseasonal and seasonal variability may be made with a 60-day cutoff. Therefore, we filtered the current data with a 60-day low-pass filter (fourth-order Butterworth). The low-passed current showed upward phase propagation that was particularly strong during June–October off Jaigarh and Bhatkal; upward phase propagation was not as striking off Goa (Figure 3b). Upward phase propagation was also evident in the high-passed current (Figure 3c). An example is the upward propagation of both equatorward and poleward current phases off Bhatkal and Jaigarh during April–June. This upward phase propagation, of which there was a hint even in the 2.5-day filtered currents (Figure 3a), indicates downward propagation of energy and is an indicator of waves propagating along the slope. Similar upward phase propagation was also seen on the shelf (Figure 2), implying the existence of propagating waves on both the shelf and slope off the Indian west coast.

4 Evidence for wave propagation on the shelf

We used wavelet coherence analysis (WCA) to examine the coherence in the shelf currents. WCA, applied to two time series that have similar spectral properties, identifies the region of strong local correlation between the time series and also gives information about the phase relationship. The WCA showed that the currents were coherent at times and the phase at a southern mooring often, but not always, led that at a northern mooring. For example, Bhatkal led Goa and Goa led Jaigarh at a period of 4 days over a large part of the record; at the 12-day period, however, Bhatkal and Goa were often in phase, while Goa led Jaigarh during July–August and lagged Jaigarh during May–June (Figure 6). This analysis shows that propagating waves should exist over a range of frequencies on the shelf on some occasions, but may not exist at all times. In other words, there exist propagation pulses, each of which may be considered an event in the context of the wavelet. The phase speeds estimated for the strong coherence at the 4-day and 12-day periods varied from 1.8 m s^{-1} to 6 m s^{-1} .

For more insight into the propagation, we examined the band-passed currents, picking the 10–14-day (called the 12-day period or band), 20–30-day (called the 25-day period or band), and 3–5-day-period (called the 4-day period or band) bands to pick the 12-day, 25-day, and 4-day peaks

seen in the wavelets. We focus on the 12-day band here in preference to the 4-day band because the QuikSCAT wind data do not permit an analysis of the forcing for the 4-day period, and in preference to the 25-day band because the latter resolves less than half as many cycles over the six-month ADCP record. The 4-day and 25-day bands are discussed briefly in Section 6.

As with the coherence, at 15 m, there was a phase lag for the 12-day period between the crests or troughs from Bhatkal to Goa and Goa to Jaigarh over some parts of the record (Figure 7b). Propagation was evident in late March and early April and again in July–August, and the time lag between the locations (~ 1 day) yielded a phase speed of $1.5\text{--}3.5\text{ m s}^{-1}$. During the summer monsoon, the currents at the three locations were practically in phase, or the current at Goa (Jaigarh) led the current at Bhatkal (Goa). The magnitude of the current did not show any pattern between the stations. Irrespective of whether there was propagation or not, an increase (decrease) in amplitude from Bhatkal to Goa was not necessarily followed by a similar increase (decrease) from Goa to Jaigarh. An example is the increase (decrease) in amplitude from Bhatkal to Goa (Goa to Jaigarh) during days 210–220 (28 July to 7 August). Propagations were weaker below 35 m.

Why is propagation evident only on some occasions? Is there no remote forcing at all at times when we see no lag in the phase of the current from south to north? Why does the phase difference between mooring pairs differ considerably on some occasions even though the inter-mooring spacing is comparable? To answer these questions, we first examined the alongshore winds derived from a daily QuikSCAT wind data set. An FFT of the winds showed peaks at periods varying from 12–40 days, and the dominant period varied with latitude. Wavelet analysis showed high energy during June for the 10–15-day period and April–May for the 35-day-period.

The band-averaged wavelet power for the 12-day period winds varied considerably in both space and time (Figure 7a). At times when propagation was evident in the current data, i. e., during late March to early April (days 82–90) and again during July–August (days 205–245) (Figure 7b), the winds were strong south of Bhatkal or up to Bhatkal, but weakened considerably to the north. Hence, the local forcing was much weaker at Goa and Jaigarh, making it possible to see a lag from south to north in the crests and troughs of the band-passed current. During the March–April event, the current data showed distinct propagation from Bhatkal to Goa, but not from Goa to Jaigarh. We attribute this apparent lack of propagation from Goa to Jaigarh to the strong local forcing north of Goa (Figure 7a), which would force at Jaigarh a strong local current that would be superimposed on the remotely forced current there. During the onset of the summer monsoon in May–June (days 140–175), the winds were strong at this frequency over much of the Indian west coast. Hence, at

all locations along the west coast till about 20°N, there was strong forcing of the current by the local winds, with result that the current at Jaigarh often led the current at Bhatkal or Goa. This strong local forcing can mask a remotely forced current. A WCA between the QuikSCAT winds and currents off Goa (figure not shown) yielded the same result. The coherence was strong during May–June, when the alongshore winds were strong over most of the coast. The local winds, however, lagged the current by 10–15 hours, suggesting a possible aliasing of the phase of the local current by a remotely forced current. (Note that the temporal resolution of the QuikSCAT wind data makes it difficult to infer much from a lag of this order.) Support to this proposition is lent by a strong coherence of the Goa current with winds south of 120°N during March and August; these winds south of the Goa mooring led the current at these times, when propagation was observed along the coast (Figure 7a). The estimated phase speed varied from 1.6 m s⁻¹ to 2.5 m s⁻¹. Similar results were obtained for the other shelf moorings.

The above analysis suggests that remote forcing must be important on the shelf off the west coast of India. This inference, as in *Shetye et al.* [2008], is based on a heuristic analysis of the wind and current data. What is not clear from this analysis is whether remote forcing exists even at those times when the local wind and current (at, say, Goa) are in phase and the current at a mooring leads that at a mooring to the south. Theory suggests that remote forcing must be present at all times, but its contribution to the current at a location will depend on the relative magnitudes of the remotely and locally forced currents. Therefore, we use CTW theory to test the hypothesis that remote forcing is present at all times on the shelf off the Indian west coast.

5 Application of CTW theory

We applied the CTW theory as described by *Brink and Chapman* [1987] to model the observed 12-day-period currents and separate the locally and remotely forced components. The wind forcing was from QuikSCAT. Details of the model may be found in earlier work on CTW theory [*Wang and Mooers*, 1976, *Huthnance*, 1978, *Brink*, 1982a,b], and we give here but a brief overview. The model calculates the modal structure and the dispersion relation for a given stratification and bottom topography for a particular region. To compute the modes, we split the west-coast shelf regime into distinct one-degree-latitude blocks (see Figure 1a), for each of which the shelf topography was prescribed from the 2-minute bathymetry of *Sindhu et al.* [2007] and the Brunt–Vaisala frequency from the one-degree temperature and salinity climatology of *Chatterjee et al.* [2012]. We assumed an

inviscid system (no horizontal friction) and constant rotation, which is reasonable for the period of interest: the critical latitude for the 12-day and 25-day period are south of the southern tip of India [Shankar and Shetye, 1997], implying that the shelf waves at these periods will remain trapped. For a coordinate system aligned with the coast such that x is positive inshore and y is positive poleward, the linearised equations for an inviscid ocean under constant rotation are as follows.

$$\begin{aligned}
u_t - fv &= \frac{-P_x}{\rho_0}; \\
v_t + fu &= \frac{-P_y}{\rho_0}; \\
P_z &= \frac{-g}{\rho}; \\
u_x + v_y + w_z &= 0; \\
\rho_t &= -w\rho_{0z}.
\end{aligned} \tag{1}$$

where u , v and w are the cross-shore, alongshore and vertical velocity components, $\rho(x, y, z, t)$ is the perturbation density from a rest state $\rho_0(z)$, and P is the perturbation pressure, and f and g are the Coriolis parameter and acceleration due to gravity, respectively. With appropriate boundary conditions, Equation (1) reduces to the following set.

$$\begin{aligned}
P_{xxt} + P_{yyt} + (f^2 + \partial_{tt})(P_z/N^2)_{zt} &= 0; \\
(f^2 + \partial_{tt})P_{zt} + N^2h_x(P_{xt} + fP_y) &= 0 \quad \text{at } z = -h(x); \\
P_{zt} + g^{-1}N^2P_t &= 0 \quad \text{at } z = 0; \\
P_{xt} + fP_y &= 0 \quad \text{at } x = 0; \\
P &\rightarrow 0 \quad \text{as } x \rightarrow -\infty,
\end{aligned} \tag{2}$$

where N^2 is the Brunt-Väisälä frequency and $h(x)$ is the local depth of the ocean. We assume the solution to be of the form

$$P = \tilde{P}(x, z) \exp[i(l y - \omega t)], \tag{3}$$

and solve numerically [Brink and Chapman, 1987] for the first three modes. The dispersion curves and eigenfunctions (cross-shelf-vertical structures) for these modes are shown in Figure 8). The dispersion curves for the three stations are similar, and so are the eigenfunctions. The 12-day and 25-day bands fall in the non-dispersive regime and the 4-day band in the dispersive regime. For the first two modes, the cross-shelf-vertical structure is barotropic on the shelf and baroclinic on

the slope; for the third mode, the shelf vertical structure is baroclinic. The shelf-edge is located roughly at 100–200 m (Figure 1a), which is at comparable to the depth of the $N^2(z)$ maxima.

Since the 12-day band falls in the non-dispersive regime, it is possible to use the longwave approximation to separate the local and remote responses [Brink, 1982a,b, Battisti and Hickey, 1984]. The pressure field can be expanded in terms of the free-wave modes

$$P(x, y, z, t) = \sum_{n=0}^{\infty} F_n(x, z)\phi_n(y, t), \quad (4)$$

where F_n is the free-wave eigenfunction for mode n , and ϕ_n can be expressed in terms of the alongshore wind stress τ and longwave phase speed c_n [Clarke, 1977, Brink, 1982a,b, Clarke and Gorder, 1986]. The equation for ϕ_n for the first mode is then

$$-\phi_{1y} + c_1^{-1}\phi_{1t} + a_{11}\phi_1 = b_1\tau_0^y, \quad (5)$$

where a_{11} is the bottom friction coefficient and b_1 the wind coupling coefficient. The normalization of b_1 is based on energy conservation for the longwave assumption [Brink, 1989]. The equation can be reduced by integrating to obtain

$$\begin{aligned} \phi(y, t) = & \phi(0, t - \int_0^y c_1^{-1} d\xi) \exp(-\int_0^y a_{11} d\xi) \\ & + \int_0^y b_1(\xi)\tau_0^y(\xi, t - \int_\xi^y c_1^{-1} d\xi') \exp(-\int_\xi^y a_{11} d\xi') d\xi \end{aligned} \quad (6)$$

where the first term on the right-hand side (RHS) is the forcing at the southern limit of the domain, given by $y = 0$, and the second term is the response due to the winds within the domain. In the calculations reported here, we assumed $y = 0$ to coincide with the southern tip of India (8.5°N) and set ϕ to zero there, which is equivalent to setting the first term on the RHS to zero. The frictional decay length scale $1/a_1$ is chosen to be larger than the characteristic wavelength, a condition necessary for the integration in Equation (6). It is to note that the pressure field is calculated only for the first mode. The calculated values of a_{11} , b_1 , and c_1 for each segment are listed in Table 2.

The alongshore velocity was estimated using the geostrophic balance

$$v = \frac{P_x}{\rho_0 f} \quad (7)$$

The modelled current was filtered to obtain the 12-day band-passed current. The CTW calculations produce a weaker current on the shelf off Jaigarh than off Goa (figure not shown) in accordance

with the observations shown in Figure 2. The reason for the weaker current off Jaigarh is the weaker wind coupling (Table 2), which is due to the widening of the shelf just south of Jaigarh (Figure 1a).

During the onset of the monsoon (May–June), the magnitudes of the observed and modelled currents were comparable off Goa (Figure 7c), but the model current led the observed current by 1 day. The contribution of individual blocks show that local forcing, which is assumed to be the contribution of the block in which the concerned mooring is located [*Brink, 1982b*], was strongest at this time (Figure 7d). The remotely forced component was significant southward of Goa till 10.5°N (block 3, Figure 7d), equatorward of which the winds were weaker (Figure 7a). The wind was also oppositely directed equatorward of 10.5°N , and the the remotely forced current at Goa due to this part of the coast was therefore opposite in phase to the local current and the remotely forced current due to the winds between Goa and 10.5°N .

There is a discrepancy in magnitude between the observed and modelled currents, but the phases are well matched. The difference in phase is of the order of a day, which may be expected because the QuikSCAT wind forcing, though available as a daily product, is based on a 3-day averaging. The magnitude difference is to be expected because the calculations have been restricted to a single mode. The pressure field is adequately described by the lowest few modes, but not the velocity. *Clarke and Gorder [1986]* and *Lopez and Clarke [1989]* estimated that it takes about 30 modes to describe the current response. Higher-order modes affect the local current component more because the wind coupling and the frictional decay length scale decrease with increasing mode number, damping the remotely forced current contribution. Therefore, adding more modes will increase the locally forced current substantially, but will not have a comparable impact on the remotely forced current, implying that the above estimate of the contribution of remote forcing is a useful approximation. We can, therefore, infer from the CTW-theory calculations that remote forcing is present all the time. When local winds are weak, as in March–April or in July–August (Figure 7a), the contribution of remote forcing to the current off, say, Goa is more important (Figure 7d). It is during the onset of the summer monsoon in May–June, when the local winds are at their peak, that the locally forced current is comparable or even stronger, but, even at this time, the contribution of remote forcing is significant. A similar conclusion holds for the other mooring locations as well.

6 Discussion

We have used current data from six ADCP moorings located on the shelf and slope off the central west coast of India to show the presence of several frequencies within the spectrum of the intraseasonal variability of the WICC. Variability was prominent in the 12-day, 25-day, and 4-day bands. Use of wavelet analysis for the winds and currents showed that local winds could not explain the observed variability in the 12-day band. Application of CTW theory confirmed that remote forcing by the winds equatorward of the mooring location contributes to the current at all times, but is more significant when the local forcing is weak, as in March–April and July–August.

In estimating the remotely forced current, we set to zero the first term on the RHS of Equation (4), implying that there is no contribution to the remotely forced current from the shelf regime beyond the west coast of India. A spatial map of the wavelet power in the 10–14 day band shows, however, that the wind is strong in the gap between India and Sri Lanka over the Gulf of Mannar (Figure 1a) and off the east coast of Sri Lanka during March–April and July–August (Figure 9), implying that the winds blowing in these regions may make a significant contribution to the remotely forced current off the central west coast. Indeed, during July–August, the winds are weak all along the west coast, forcing a weak local and remote current (Figure 7c,d), suggesting that the stronger winds (Figure 9) off Tuticorin (see Figure 1a for location) in the Gulf of Mannar is the more likely source of the current at Goa; that the Tuticorin wind is roughly in phase with the observed current off Goa (Figure 7e) strengthens this hypothesis. During monsoon onset in May–June, the Tuticorin winds are opposite in phase (Figure 7e), and may contribute to weakening the remotely forced current. In summary, it is likely that remotely forced shelf waves from the Gulf of Mannar, or even from the east coast of Sri Lanka may affect the shelf WICC.

Wavelet analysis and band-pass filtering of the data showed only one propagation event at the 25-day period (figure not shown). Wavelet analysis of the wind showed moderate-to-strong winds in this band along the entire west coast over most of the record, the exception being July. The observed 25-day current was not, however, significantly weaker during July, suggesting again the possibility of remote forcing from beyond the west coast.

Even at a period as short as 4 days, there were many propagation events (Figure 10a-d). Unlike at the higher periods of 12 and 25 days, propagation was seen even during the summer monsoon, with four distinct events during June–August (Figure 10c). At this period, propagation was seen even at deeper depths. This remote forcing at the 4-day period contradicts the inference of *Shetye*

et al. [2008], who used a month-long record of currents from the inner shelf off Goa to infer the presence of remote forcing at periods exceeding 10 days, but found a strong correlation between the local wind and current at shorter periods. Shetye *et al.* also found a 4-day period in the data and attributed currents at such periods shorter than 10 days to local forcing. The ADCP data were collected on the outer shelf, in a water-column depth of $\tilde{100}$ m, but they show evidence for remote forcing even at the 4-day period. That such propagation was not discernible at the 4-day period in the *Shetye et al.* [2008] data set suggests that the 2003 current-meter data must have been collected at a time when the local winds off Goa were strong enough to mask completely the effect of any propagating wave. If the ADCP record had been restricted to a short duration around day 220, when propagation is seen for the 12-day period (Figure 7b), but not for the 4-day period (Figure 10b), then an inference similar to that of *Shetye et al.* [2008] could have been drawn. It is the longer period of observation that allowed us to distinguish between the times when propagation is distinctly seen from times when it must exist, but is masked by strong local forcing. The analysis suggests that a high correlation between local winds and currents does not rule out a remotely forced contribution to the current.

On the slope, the first ADCP bin for which we could analyse propagation is centred at 55 m; data were not available closer to the surface owing to echoes. Unlike on the shelf, no evidence of propagating waves was found on the slope for the 12-day and 25-day bands, but there were several events for the 4-day band (Figure 10b,d). Propagation in the 4-day band was also observed in the deeper layers up to 120 m.

A depth-time plot of the wavelet power for the 12-day band showed simultaneous occurrence of high-amplitude currents on the shelf, particularly off Bhatkal and Goa (figure not shown), but not on the slope (Figure 11). On the slope, the strong currents occurred at different times and depths at the three locations. In other words, the alongshore current at this period is coherent along the shelf, but decorrelates rapidly along the slope. The result is similar for the 25-day band (figure not shown), in which too there is a lack of coherence among the slope moorings.

This alongshore decorrelation over just 200–400 km is in marked contrast to the alongshore coherence of the seasonal WICC (Figure 1c,d). For the East India Coastal Current (EICC) [*Shankar et al.*, 1996, *McCreary et al.*, 1996] a similar decorrelation was noted by *Durand et al.* [2009] in the geostrophic currents estimated from along-track altimeter data. They too noted the contrast between the coherence evident at the seasonal time scale and the rapid alongshore decorrelation at intraseasonal periods. One possible reason for such a rapid alongshore decorrelation could be

alongshore variation in winds, evident in the wavelet analysis of the QuikSCAT winds (Figure 7a). Another possible reason is the downward propagation of energy in the form of coastal Kelvin beams, which have been predicted by linear wave theory to bend as much as 350 m over the 15°-long Indian west coast (5-20°N) at a period of 30 days [Nethery and Shankar, 2007]. Since the bending of the beam increases with frequency, it is possible that a 12-day-period current observed at ~ 40 m at Bhatkal can be traced to deeper depths off Goa and may have been missed by the Goa slope ADCP because data are not available below ~ 170 m. Note, however, that data on the slope are restricted to depths below 55 m. On the shelf too, at these depths, propagation was evident only for the 4-day period, but not for the higher periods. It is possible that a similar situation may exist on the slope too: if data were available closer to the surface, would propagating waves have been seen at higher periods? In both cases, whether bending of beams or propagating waves at higher periods near the surface, it is important to sample as much of the water column as is possible.

The seasonal cycle of the WICC on the slope has been linked to forcing by winds blowing along the east coast of India [McCreary *et al.*, 1993, Shankar and Shetye, 1997, Shankar *et al.*, 2002]. The Kelvin wave that links the seasonal cycle of the EICC and WICC goes round the southern tip of Sri Lanka, and the numerical models barely resolve the Gulf of Mannar. Altimeter along-track data indicate that the boundary-trapped current in the region bypasses, or "does not see", the Gulf of Mannar, with the maximum in the EICC shifting offshore for the track passing through the Gulf of Mannar, unlike with the EICC off the Indian east coast, for which the maximum occurs near the coast [Durand *et al.*, 2009]. The wavelength of these waves is large and they are not affected by this small bend in the coastline. In contrast, since the CTW has to follow the shelf, the shelf forcing from beyond the southern tip of India would have to be traced back along the coast of the Gulf of Mannar, implying that forcing by the strong Gulf-of-Mannar winds may be important for the shelf WICC.

It is pertinent to note that the propagating waves described in this paper, or the propagating waves inferred by Shetye *et al.* [2008], are primarily on the west-coast shelf, of whose dynamics we know much less than that of the slope. The theoretical studies mentioned above for the large-scale circulation were focussed largely on the seasonal time scales and restricted to the boundary currents trapped against the shelf-break. All of them have invoked long, baroclinic waves to explain the observed circulation. The ADCP observations presented here, and the altimeter-data-analysis of Durand *et al.* [2009], suggest that a description of the intraseasonal variability of the WICC and EICC may require measurement of currents over the entire water column or ADCP moorings

located much closer than the 200-km spacing of this study.

The analysis presented here does, however, bear out the importance of making long-term current observations on the shelf off the Indian coast. This paper presents the first description of the intraseasonal variability of the shelf WICC, and the success of CTW theory, applied for the first time in the North Indian Ocean, suggests that it is important to ensure that these current measurements on the shelf continue in spite of the problems posed by fishing in the region. Just as the hydrographic cruises in the Indian Exclusive Economic Zone in the 1980s and 1990s [*Shetye et al.*, 1990, 1991, *Shetye and Gouveia*, 1998] motivated a series of modelling studies that invoked linear wave theory to yield insights into the seasonal cycle of the large-scale circulation in the Indian Ocean, data from these shelf moorings will lead to significant advances in our understanding of shelf circulation, which is important for the biogeochemistry of the region.

7 Acknowledgments

The CTW theory presented in this paper was provoked by the critical comments of Dr. Barbara Hickey and an anonymous reviewer; inclusion of this analysis improved the manuscript significantly, and we are grateful to the reviewers. We are also grateful to Dr. Kenneth Brink and the late Dr. David Chapman for making their CTW codes public. Dr. Allan Clarke and Dr. Brink helped us get these codes and we are grateful to Dr. Brink for helping us understand the code outputs. We thank USGS for providing the ADCP data processing toolbox (http://woodshole.er.usgs.gov/operations/stg/pubs/ADCPtools/adcp_index.htm). The MATLAB version of the toolbox was converted to Octave and C by A. Krishnakiran, R. Fernandes, N. Nasnodkar, and S.P. Vernekar. K. Kutsuwada helped us with filling of data gaps and Teledyne RD Instruments provided technical support. The FORTRAN code for wavelet analysis and the R package for wavelet coherence spectra were downloaded from <http://paos.colorado.edu/research/wavelets/> and <http://tocsy.agnld.uni-potsdam.de/wavelets/>, respectively. All figures in this paper were made using Generic Mapping Tools and the analysis was done using Ferret. We also thank the officers, crew, and seamen on the mooring cruises for providing the necessary support for deploying the ADCPs. Financial support for this work was provided by CSIR and INCOIS (Ministry of Earth Sciences). Amol Prakash thanks CSIR for his research fellowship. This is NIO contribution 0000.

Table 1: Mooring details^a

ADCP No.	Mooring type	Mooring location	Position	ADCP depth(m)	Water depth (m)	Angle ^c (deg)	Start date (2008)	End date (2008)
J100	Shelf	Jaigarh	17.15°N, 72.08°E	92	108	20	04 Mar	18 Oct
J1000	Slope	Jaigarh	17.26°N, 71.48°E	439	1078	44	03 Mar	20 Oct
G100	Shelf	Goa	15.17°N, 73.19°E	90	98	14	02 Mar	22 Oct
G1000 ^b	Slope	Goa	15.21°N, 72.70°E	171	1005	7	07 Mar	16 Sep
B100	Shelf	Bhatkal	13.67°N, 73.51°E	97	104	-1	05 Mar	07 Sep
B1000	Slope	Bhatkal	13.60°N, 73.24°E	378	1050	8	05 Mar	15 Oct

^a All ADCPs are upward looking. 75 kHz RDI ADCPs were used for slope mooring and 300 kHz RDI ADCPs were used for shelf mooring. ^b A seventh ADCP had been deployed at a depth of about 350 m a few miles away from the slope ADCP off Goa, but it malfunctioned and did not record any data. The ADCP that recorded data on the slope off Goa, G1000, had been deployed to examine how the currents changed in the top 30–40 m below the surface. This attempt was made because the upward-looking ADCPs do not yield data in the last 10% of their range, and it was considered desirable to check for the near-surface vertical shear. The data in the top 10% of the range from the surface are removed because surface echoes due to surface waves and winds contaminate the measurement. This slope ADCP off Goa recorded data only till September, as did the shelf ADCP off Bhatkal. ^c The currents are rotated anticlockwise in Cartesian coordinate system to estimate the alongshore component.

Table 2: Model parameter details for the different blocks shown in Figure 1a. Block B5, B7, and B9 represent the Bhatkal, Goa and Jaigarh mooring locations

Blocks	c_1 (m s ⁻¹)	b_1 (cm ^{-1/2} s ^{-1/2})	a_{11} (cm) × 10 ⁹
B1	2.03	2.17	3.14
B2	2.43	1.95	2.22
B3	1.83	2.46	5.64
B4	2.75	2.37	4.11
B5	2.89	1.99	2.81
B6	3.75	2.48	4.15
B7	3.90	2.14	3.02
B8	3.57	2.07	3.30
B9	4.43	1.84	1.98

References

- Antony, M., and S. Shenoi, On the flow, thermal field and winds along the western continental shelf of India, *Cont. Shelf Res.*, *13*, 425–439, 1993.
- Aparna, M., S. R. Shetye, D. Shankar, S. S. C. Shenoi, P. Mehra, and R. G. P. Desai, Estimating the seaward extent of sea breeze from QuikSCAT scatterometry, *Geophys. Res. Lett.*, *32*, L13601, doi:10.1029/2005GL023107, 2005.
- AVISO, Aviso user handbook: Merged TOPEX/Poseidon products, *Tech. rep.*, Toulouse, France, 1996.
- Battisti, D. S., and B. M. Hickey, Applications of remote wind forced coastal trapped wave theory to the Oregon and Washington coasts, *J. Phys. Oceanogr.*, *14*, 1984.
- Bell, C., J. Vassie, and P. Woodworth, Pol-PSMSL Tidal Analysis Software Kit 2000 (TASK-2000), *Tech. rep.*, Proudman Oceanogr. Lab., Bidston Observatory, Merseyside, U.K., 1998.
- Brink, K. H., The effect of bottom friction on low-frequency coastal trapped waves, *J. Phys. Oceanogr.*, *12*, 1982a.
- Brink, K. H., A comparison of long coastal-trapped wave theory with observations off Peru, *J. Phys. Oceanogr.*, *12*, 1982b.
- Brink, K. H., Energy conservation in coastal-trapped wave calculations, *J. Phys. Oceanogr.*, *19*(7), 1011–1016, 1989.
- Brink, K. H., and D. C. Chapman, Programs for computing properties of coastal-trapped waves and wind driven motions over the continental shelf and slope, *Tech. rep.*, Woods Hole Oceanographic Institution, 1987.
- Bruce, J., D. R. Johnson, and J. C. Kindle, Evidence for eddy formation in the eastern Arabian Sea during the northeast monsoon, *J. Geophys. Res.*, *99*, 76517664, 1994.
- Chatterjee, A., D. Shankar, S. S. C. Shenoi, G. V. Reddy, M. Ravichandran, V. V. Gopalkrishna, E. P. R. Rao, T. V. S. U. Bhaskar, and V. N. Sanjeevan, A new atlas of temperature and salinity for the North Indian Ocean, *J. Earth Syst. Sci.*, *In press*, 2012.

- Church, J. A., H. J. Freeland, and R. L. Smith, Coastal trapped waves on the Australian continental shelf. Part I: Propagation of modes, *J. Phys. Oceanogr.*, *16*, 1929–1943, 1986.
- Clarke, A. J., Observational and numerical evidence for wind-forced coastal trapped long waves, *J. Phys. Oceanogr.*, *7*, 231–247, 1977.
- Clarke, A. J., Origin of the coastally trapped waves observed during the Australian Coastal Experiment, *J. Phys. Oceanogr.*, *17*, 1847–1859, 1987.
- Clarke, A. J., and S. V. Gorder, A method for estimating wind-driven frictional time-dependent, stratified shelf and slope water flow, *J. Phys. Oceanogr.*, *16*, 1986.
- DeTracey, B., C. Tang, and P. Smith, Low-frequency currents at the northern shelf edge of the Grand Banks, *J. Geophys. Res.*, *101*, 14,223–14,235, 1996.
- Durand, F., S. R. Shetye, J. Vialard, D. Shankar, S. S. C. Shenoi, C. Ethe, and G. Madec, Impact of temperature inversions on SST evolution in the south-eastern Arabian Sea during the pre-summer monsoon season, *Geophys. Res. Lett.*, *31*, L01305, doi:10.1029/2003GL018906, 2004.
- Durand, F., D. Shankar, C. de Boyer Montgut, S. S. C. Shenoi, B. Blanke, and G. Madec, Modeling the barrier-layer formation in the south-eastern Arabian Sea, *J. Climate*, *20*, 2109–2120, 2007.
- Durand, F., D. Shankar, F. Birol, and S. S. C. Shenoi, Spatiotemporal structure of the East India Coastal Current from satellite altimetry, *Geophys. Res. Lett.*, *114*, C02013, doi:10.1029/2008JC004807, 2009.
- Freeland, H. J., F. M. Boland, A. J. Church, A. M. G. Forbes, R. L. Huyer, R. L. Smith, R. O. R. Y. Thompson, and N. J. White, The Australian Coastal Experiment: A search for coastal-trapped waves, *J. Phys. Oceanogr.*, *16*, 1230–1249, 1986.
- Hamon, B. V., Continental shelf waves and the effects of atmospheric pressure and wind stress on sea level, *J. Geophys. Res.*, *71*, 1966.
- Hickey, B., E. L. Dobbins, and S. E. Allen, Local and remote forcing of currents and temperature in the central Southern California Bight, *J. Geophys. Res.*, *108(C3)*, 3081, doi:10.1029/2000JC000313, 2003.

- Hickey, B. M., The fluctuating longshore pressure gradient on the Pacific northwest shelf: A dynamical analysis, *J. Phys. Oceanogr.*, *14*, 276–293, 1984.
- Hickey, B. M., R. E. Thomson, H. Yih, and P. H. Leblond, Velocity and temperature fluctuations in a buoyancy-driven current off Vancouver Island, *J. Geophys. Res.*, *96*, 10,507–10,538, 1991.
- Huthnance, J. M., On coastal trapped waves: Analysis and numerical calculations by inverse iterations, *J. Phys. Oceanogr.*, *8*, 1978.
- Kumar, P. D., and K. Srinivas, Variability in measured current structure on the southwest continental shelf of India, *J. Coastal Res.*, *23*(3), 647–657, 2007.
- Kumar, P. H., and N. M. Kumar, On the flow and thermohaline structure off Cochin during pre-monsoon season, *Cont. Shelf Res.*, *16*(4), 457–468, 1996.
- Kurian, J., and P. N. Vinayachandran, Mechanisms of formation of Arabian Sea mini warm pool in a high resolution ogcm, *J. Geophys. Res.*, *112*, C05009, doi:10.1029/2006JC003631, 2007.
- Lopez, M., and A. Clarke, The wind-driven shelf and slope water flow in terms of a local and remote response, *J. Phys. Oceanogr.*, *19*, 1092–1101, 1989.
- Maiwa, K., Y. Masumoto, and T. Yamagata, Characteristic of coastal trapped waves along the southern and eastern coasts of Australia, *J. Oceanogr.*, *66*, 2010.
- Mariano, A. J., E. H. Ryan, B. D. Perkins, and S. Smithers, The Mariano Global Surface Velocity Analysis 1.0, *Uscg report cg-d-34-95*, Office of Engineering, Logistics, and Development, U.S. Coast Guard, 1995.
- Martinez, J. A., and J. S. Allen, A modelling study of coastal-trapped wave propagation in the Gulf of California. part 1: Response to remote forcing, *J. Phys. Oceanogr.*, *31*, 1313–1331, 2004.
- McCreary, J., P. K. Kundu, and R. L. Molinari, A numerical investigation of the dynamics, thermodynamics and mixed-layer processes in the Indian Ocean, *Prog. Oceanogr.*, *31*, 181–244, 1993.
- McCreary, J., W. Han, D. Shankar, and S. R. Shetye, Dynamics of the East India Coastal Current: 2. Numerical solutions, *J. Geophys. Res.*, *101*, 13,993–14,010, 1996.
- Middleton, J. F., and D. G. Wright, Coastal-trapped waves on the Labrador Shelf, *J. Geophys. Res.*, *96*, 2599–2617, 1991.

- Middleton, J. H., and A. Cunningham, Wind-forced continental shelf waves from geographical origin, *Cont. Shelf Res.*, *3*, 215–232, 1984.
- Mitchum, G. T., and A. J. Clarke, Evaluation of frictional wind forced long wave theory on west Florida Shelf, *J. Phys. Oceanogr.*, *16*, 1029–1037, 1986.
- Miyama, T., J. P. McCreary, D. Sengupta, and R. Senan, Dynamics of biweekly oscillations in the Equatorial Indian Ocean, *J. Physic. Oceanogr.*, *36*, 827–846, 2006.
- Mysak, L. A., Recent advances in shelf wave dynamics, *Rev. Geophys. Space Phys.*, *18*, 211–241, 1980.
- Nethery, D., and D. Shankar, Vertical propagation of baroclinic Kelvin waves along the west coast of india, *J. Earth Syst. Sci.*, *4*, 311–339, 2007.
- Ogata, T., H. Sasaki, V. S. N. Murty, M. S. S. Sarma, and Y. Masumoto, Intraseasonal meridional current variability in the eastern Equatorial Indian Ocean, *J. Geophys. Res.*, *113*, C07037, doi:10.1029/2007JC004331, 2008.
- Schott, F. A., and J. P. McCreary, The monsoon circulation of the indian ocean, *Prog. Oceanogr.*, *51*, 1–120, 2001.
- Sengupta, D., R. Senan, V. S. N. Murty, and V. Fernando, A biweekly in the equatorial indian ocean, *J. Geophys. Res.*, *109*, C10003, doi:10.1029/2004JC002329, 2004.
- Shankar, D., and S. R. Shetye, On the dynamics of the Lakshadweep high and low in southeastern Arabian Sea, *J. Geophys. Res.*, *102*, 12,551–12,562, 1997.
- Shankar, D., J. McCreary, W. Han, and S. R. Shetye, Dynamics of the East India Coastal Current: 1. Analytic solutions forced by interior Ekman pumping and local alongshore winds, *J. Geophys. Res.*, *101*, 13,975–13,991, 1996.
- Shankar, D., P. N. Vinayachandran, and A. S. Unnikrishnan, The monsoon currents in the North Indian Ocean, *Prog. Oceanogr.*, *52*, 63–120, 2002.
- Shenoi, S. S. C., and M. K. Antony, Current measurements over the western continental shelf of India, *Cont. Shelf Res.*, *11(1)*, 81–93, 1991.

- Shenoi, S. S. C., M. K. Antony, and D. Sundar, Nature of the observed oscillatory flows in shelf waters of the western continental shelf of India, *J. Coastal Res.*, 4(4), 617–626, 1998.
- Shenoi, S. S. C., P. Saji, and A. Almeida, Near-surface circulation and kinetic energy in the tropical Indian Ocean derived from Lagrangian drifters, *J. Mar. Res.*, 57, 885–907, 1999.
- Shetye, S. R., and A. D. Gouveia, Coastal circulation in the North Indian Ocean. Coastal segment (14,S-W), *The Sea*, 11, 523–556, 1998.
- Shetye, S. R., A. D. Gouveia, S. S. C. Shenoi, D. Sundar, G. S. Michael, A. M. Almeida, and K. Santanam, Hydrography and circulation off the west coast of India during the southwest monsoon 1987, *J. Mar. Res.*, 48, 359–378, 1990.
- Shetye, S. R., A. D. Gouveia, S. S. C. Shenoi, G. S. Michael, D. Sundar, A. M. Almeida, and K. Santanam, The coastal current off western India during the northeast monsoon, *Deep Sea Res., Part I*, 38, 1517–1529, 1991.
- Shetye, S. R., A. D. Gouveia, and S. S. C. Shenoi, Circulation and water masses of the Arabian Sea, Biochemistry of the Arabian Sea, Present information and gaps, *Proc. Indian Acad. Sci. (Earth Planet. Sci.)*, 1994.
- Shetye, S. R., I. Suresh, D. Shankar, D. Sundar, S. Jayakumar, P. Mehra, R. G. Prabhudesai, and P. S. Pednekar, Observational evidence for remote forcing of the West India Coastal Current, *J. Geophys. Res.*, 113, C11001, doi:10.1029/2008JC004874, 2008.
- Sindhu, B., I. Suresh, A. Unnikrishnan, N. Bhatkar, Neetu, and G. Michael, Improved bathymetric datasets for the shallow water regions in the Indian Ocean, *J. Earth Syst. Sci.*, 116, 261–274, 2007.
- Smith, R. L., Poleward propagating disturbances in currents and sea level along the Peru coast, *J. Geophys. Res.*, 83, 6083–6092, 1984.
- Stramma, L., J. Fischer, and F. Schott, The flow field off southwest India at 8N during the southwest monsoon of August 1993, *J. Mar. Res.*, 54, 55–72, 1996.
- Unnikrishnan, A. S., and M. Antony, On vertical velocity fluctuations and internal tides in an upwelling region off the west coast of India, *Est. Coast. Shelf Sci.*, 31, 865–873, 1990.

- Varkey, M. J., Power spectra of currents off Bombay, *Indian J. Mar. Sci.*, 9, 278–280, 1980.
- Vialard, J., S. Shenoi, J. McCreary, D. Shankar, F. Durand, V. Fernando, and S. Shetye, Intraseasonal response of the Northern Indian Ocean coastal waveguide to the Madden-Julian oscillation, *Geophys. Res. Lett.*, 36, L14606, doi:10.1029/2009GL038450, 2009.
- Wang, D. P., and C. N. Mooers, Coastal-trapped waves in a continuously stratified ocean, *J. Phys. Oceanogr.*, 6, 1976.
- Wilkin, J. L., and D. C. Chapman, Scattering of continental shelf waves at a discontinuity in shelf width, *J. Phys. Oceanogr.*, 17(6), 713–724, 1987.
- Wyrтки, K., Oceanographic atlas of the International Indian Ocean Expedition, *Washington D. C.: National Science Foundation*, 1971.

8 Captions

Figure 1. (a) The west coast of India showing the locations of ADCP moorings. Mooring B1000, G1000, and J1000 were on the slope at 1000 m water depth, and moorings B100, G100, and J100 were on the shelf at 100 m water depth. The dashed line divides the coast into 9 blocks of 1° each from B1 (8.5°N) to B9 (17.5°N). The bathymetry is from *Sindhu et al.* [2007]. (b) The location of region of interest in the Indian Ocean. (c) Monthly climatology of alongshore currents from ship drifts [*Mariano et al.*, 1995]. (d) Weekly climatology of geostrophic current calculated from merged altimetry (TOPEX/Poseidon and ERS1/2) data set [*AVISO*, 1996].

Figure 2. 2.5-day low-passed and detided alongshore currents (positive poleward) at Jaigarh (top), Goa (middle), and Bhatkal (bottom) on the slope (left) and the shelf (right). The white space implies data are not available and the dashed line shows the 55 m (15 m) water column depth on the slope (shelf).

Figure 3. Alongshore currents from the Bhatkal and Jaigarh slope moorings. (a) 2.5-day low-passed currents. (b) 60-day low-passed currents. (c) 60-day high-passed currents. The dashed line shows the 55 m water column depth at slope.

Figure 4. First two EOF modes for (a) shelf and (b) slope moorings. The left (right) panel shows the temporal (spatial) vector. The variance for each mode is included in the left panel. Mode 1 (Mode 2) shown in black (red).

Figure 5. Morlet wavelet power spectra for alongshore currents off Jaigarh (top), Goa (middle), and Bhatkal (bottom) for the slope moorings at 55 m depth (left) and shelf moorings at 15 m depth (right). The thick black lines show the cone of influence (COI) for the wavelet power spectra. The dashed line highlights the 4-day, 12-day and 25-day periods.

Figure 6. Wavelet coherence for the shelf mooring. The contour line shows 5% significance level against red noise. The arrows show the relative phase relationship with in-phase (anti-phase) pointing right (left). The first station leads (lags) the second station in anticlockwise direction (clockwise). For example, during March–April in the top panel, Goa leads Jaigarh by 90 degrees (1-day) for the 4-day period. The arrows are shown only for values greater than 0.5. The thick black lines show the COI. The dashed lines mark the 4 day, 12 day and 25 periods.

Figure 7. Observed current from the shelf moorings, QuikSCAT alongshore wind, and modelled (CTW theory) current for the 12-day band. (a) QuikSCAT wind wavelet as a function of latitude (along the coast) and time. The thick black lines show the mooring location. (b) Band-passed cur-

rent off Bhatkal (black), Goa (red), and Jaigarh (green) at 15 m depth. The shaded region denotes the period when free wave propagation is observed between the three stations. (c) Comparison between observed current off Goa (black) and modelled (CTW theory) current (red). The locally forced current is also shown (green); the remote contribution is the difference between the modelled and local currents. (d) Modelled local (black) current at Goa (B7) and remote contributions from different blocks: B5 (red), B3 (green), and B1 (blue). (e) Observed current off Goa (black) and QuikSCAT winds (ms^{-1}) at each latitude: Tuticorin (red), 8.5°N (green), 10.5°N (blue), and 12.5°N (orange). The amplitude of winds were multiplied by a factor of 3. Note that a positive wind is downwelling-favourable: hence, the Tuticorin wind is positive if the meridional component is equatorward.

Figure 8. Results of the CTW calculations. (a) Dispersion curve for the first three CTW modes for Bhatkal (black), Goa (red) and Jaigarh (green). (b)–(d) Offshore-vertical structure for the first three modes at Goa; the structure is similar at the other two locations.

Figure 9. Spatial variation of the wavelet power at the 12-day period for the meridional component of the QuikSCAT winds. In each panel, the wavelet power was averaged over a month. The wavelet power is plotted on a \log_2 scale.

Figure 10. 3–5-day band-passed currents for Bhatkal (black), Goa (red), and Jaigarh (green). The shaded region denotes the period when free wave propagation is observed between the three stations. (a) Shelf current at 15 m during March–May. (b) Slope current at 55 m during March–May (c) Shelf current at 15 m during June–August (d) Slope current at 55 m during June–August.

Figure 11. Band-averaged wavelet power spectra of alongshore currents on the slope off Jaigarh (top), Goa (middle), and Bhatkal (bottom) as a function of time and depth for the 12-day period. The dashed line shows the 55 m water column depth on the slope.

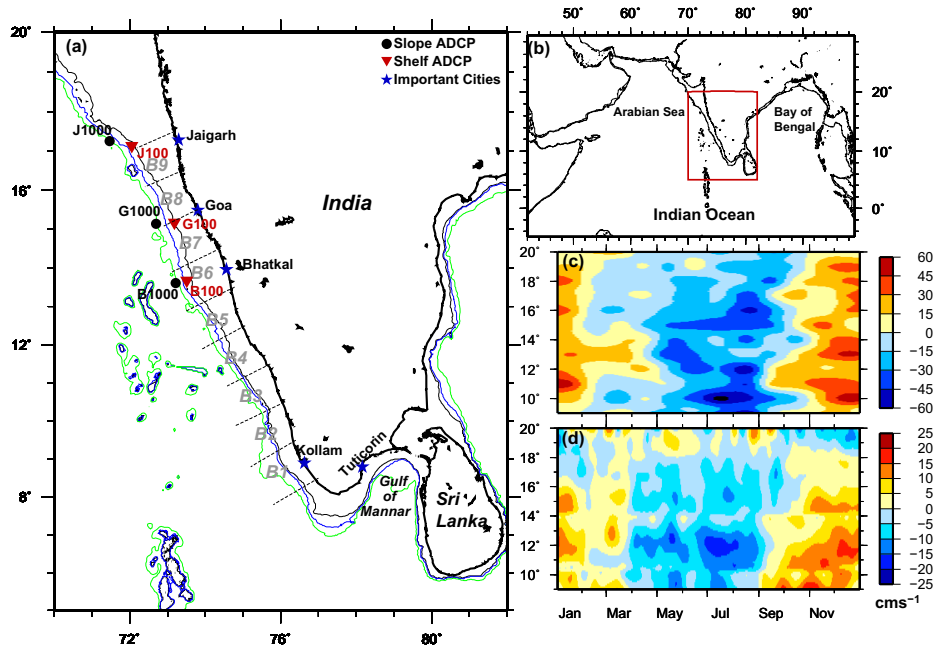


Figure 1: (a) The west coast of India showing the locations of ADCP moorings. Mooring B1000, G1000, and J1000 were on the slope at 1000 m water depth, and moorings B100, G100, and J100 were on the shelf at 100 m water depth. The dashed line divides the coast into 9 blocks of 1° each from B1 (8.5°N) to B9 (17.5°N). The bathymetry is from *Sindhu et. al.* [2007]. (b) The location of region of interest in the Indian Ocean. (c) Monthly climatology of alongshore currents from ship drifts [*Mariano et. al.*,1995]. (d) Weekly climatology of geostrophic current calculated from merged altimetry (TOPEX/Poseidon and ERS1/2) data set [*AVISO*, 1996].

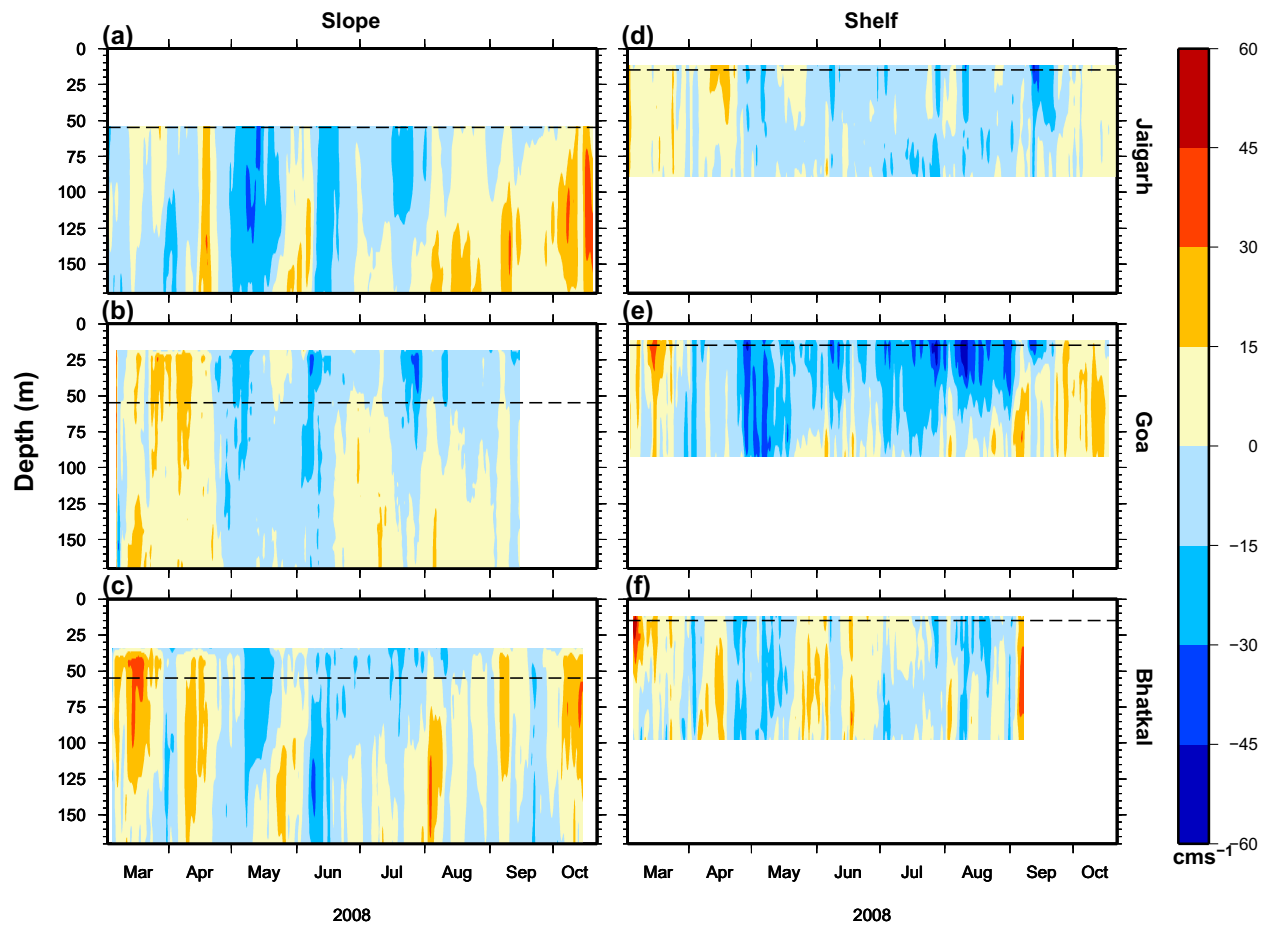


Figure 2: 2.5-day low-passed and detided alongshore currents (positive poleward) at Jaigarh (top), Goa (middle), and Bhatkal (bottom) on the slope (left) and the shelf (right). The white space implies data are not available and the dashed line shows the 55 m (15 m) water column depth on the slope (shelf).

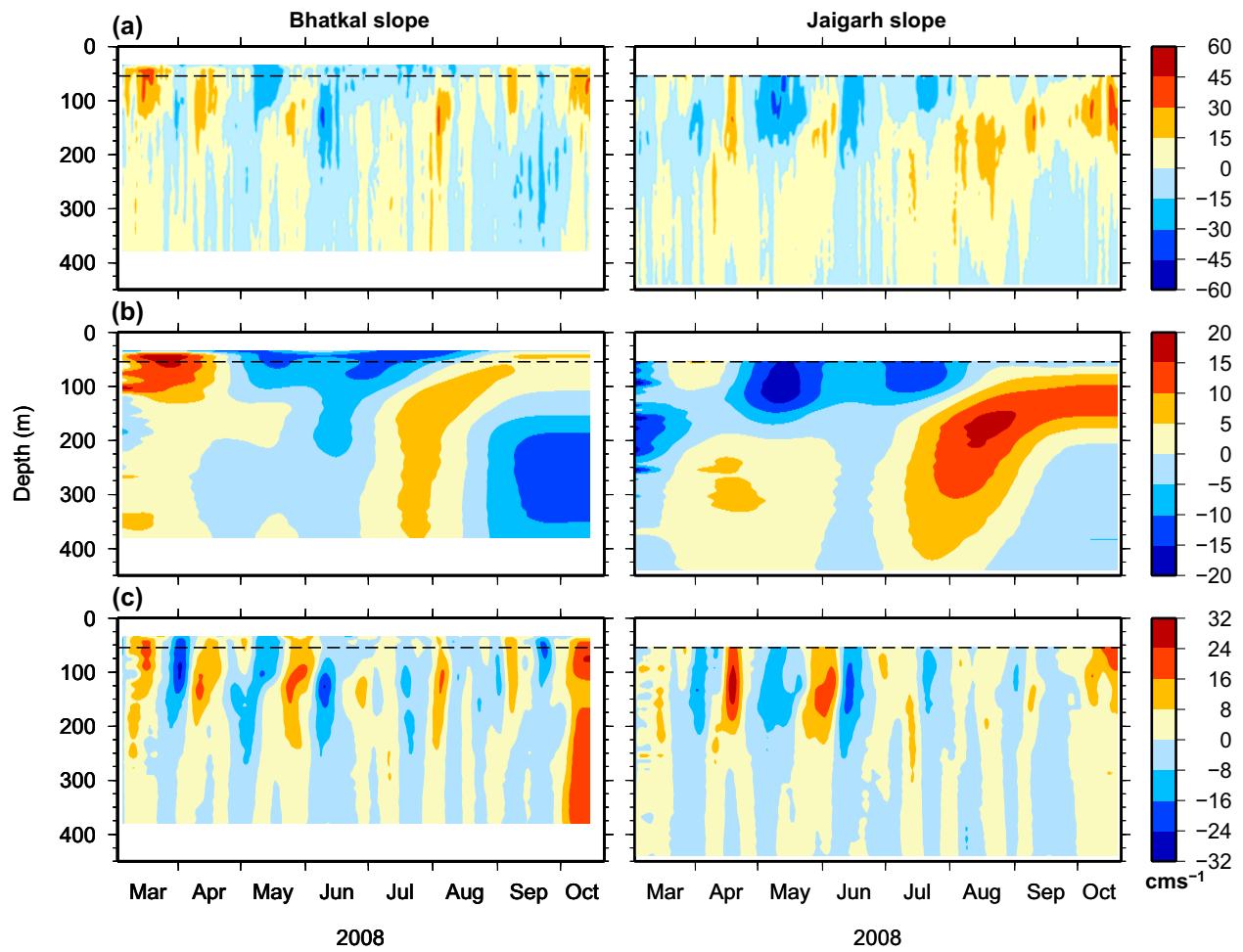


Figure 3: Alongshore currents from the Bhatkal and Jaigarh slope moorings. (a) 2.5-day low-passed currents. (b) 60-day low-passed currents. (c) 60-day high-passed currents. The dashed line shows the 55 m water column depth at slope.

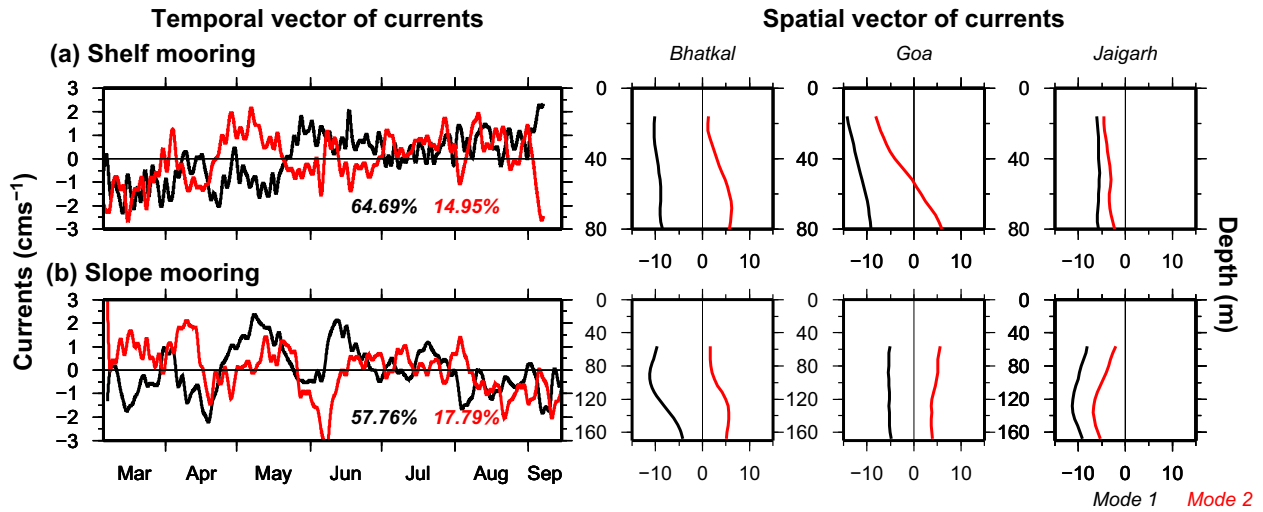


Figure 4: First two EOF modes for (a) shelf and (b) slope moorings. The left (right) panel shows the temporal (spatial) vector. The variance for each mode is included in the left panel. Mode 1 (Mode 2) shown in black (red).

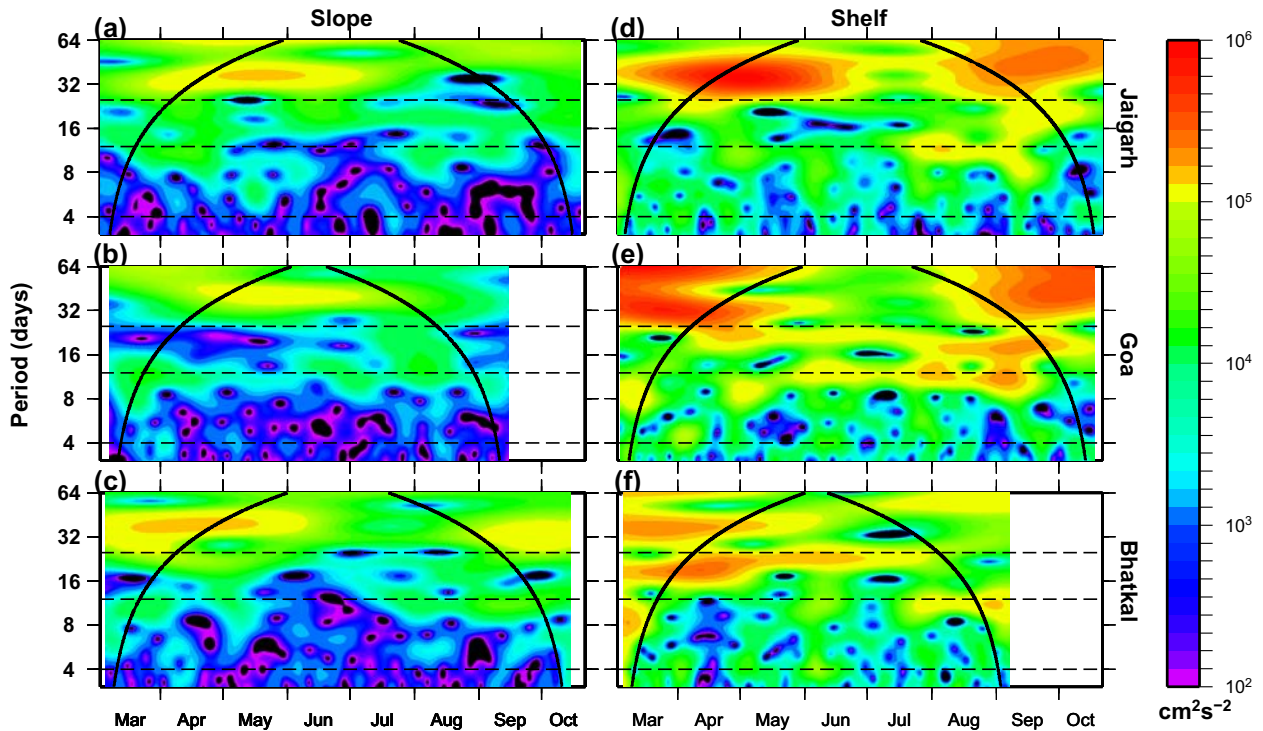


Figure 5: Morlet wavelet power spectra for alongshore currents off Jaigarh (top), Goa (middle), and Bhatkal (bottom) for the slope moorings at 55 m depth (left) and shelf moorings at 15 m depth (right). The thick black lines show the cone of influence (COI) for the wavelet power spectra. The dashed line highlights the 4-day, 12-day and 25-day periods.

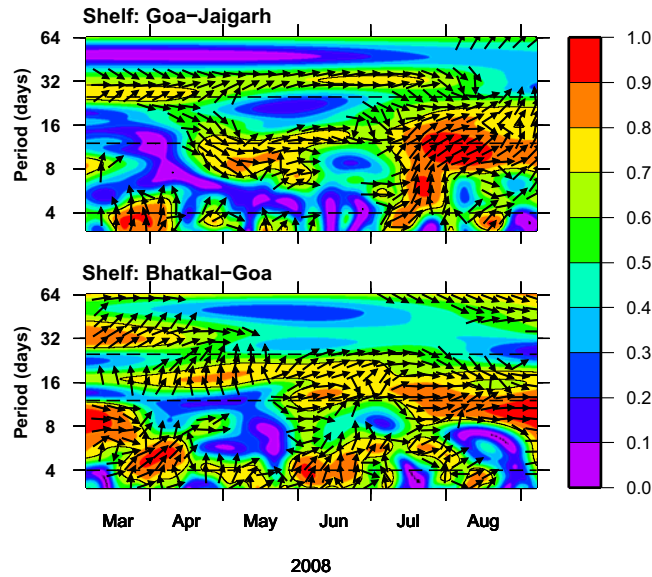


Figure 6: Wavelet coherence for the shelf mooring. The contour line shows 5% significance level against red noise. The arrows show the relative phase relationship with in-phase (anti-phase) pointing right (left). The first station leads (lags) the second station in anticlockwise direction (clockwise). For example, during March–April in the top panel, Goa leads Jaigarh by 90 degrees (1-day) for the 4-day period. The arrows are shown only for values greater than 0.5. The thick black lines show the COI. The dashed lines mark the 4 day, 12 day and 25 periods.

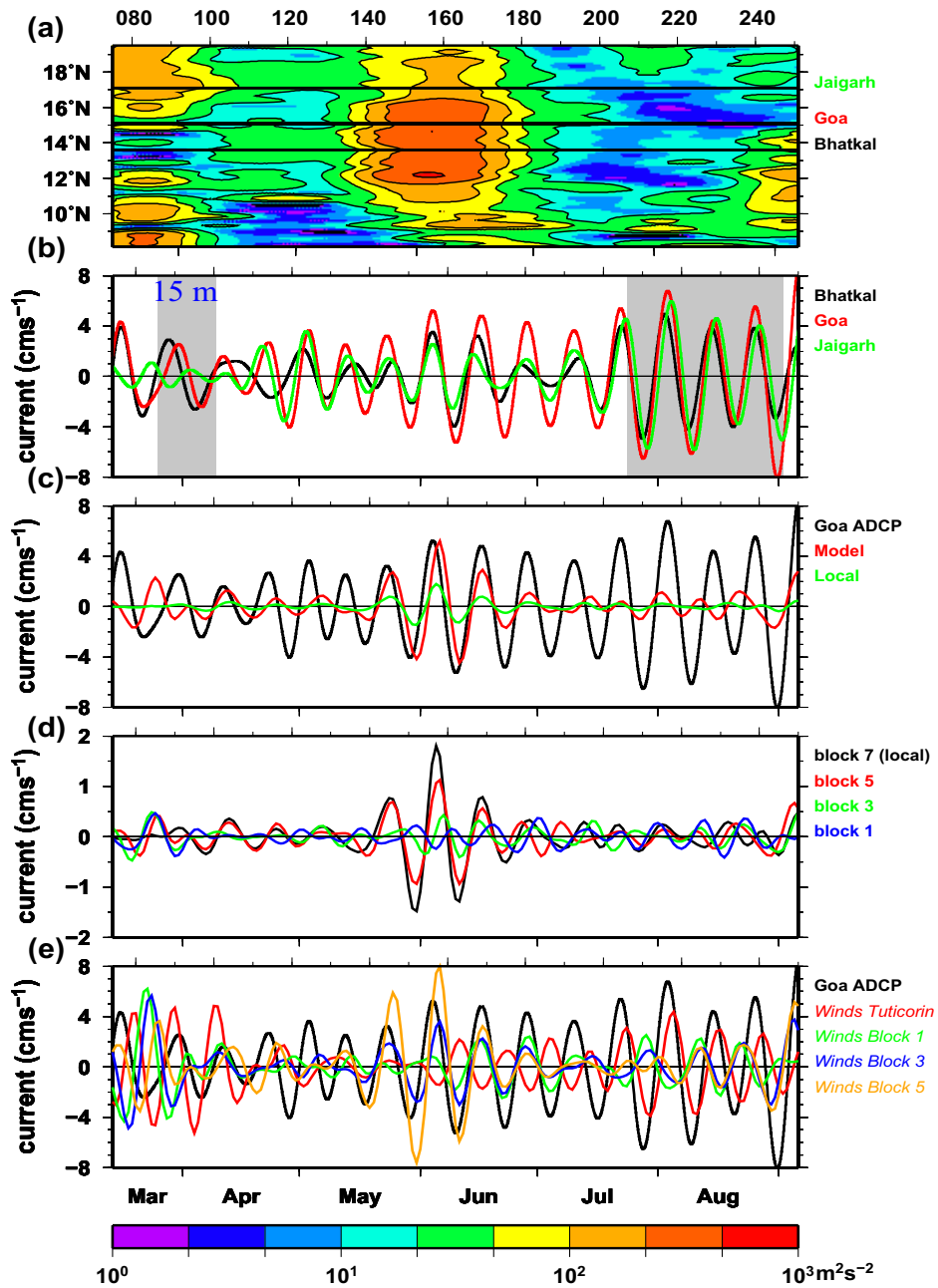


Figure 7: Observed current from the shelf moorings, QuikSCAT alongshore wind, and modelled (CTW theory) current for the 12-day band. (a) QuikSCAT wind wavelet as a function of latitude (along the coast) and time. The thick black lines show the mooring location. (b) Band-passed current off Bhatkal (black), Goa (red), and Jaigarh (green) at 15 m depth. The shaded region denotes the period when free wave propagation is observed between the three stations. (c) Comparison between observed current off Goa (black) and modelled (CTW theory) current (red). The locally forced current is also shown (green); the remote contribution is the difference between the modelled and local currents. (d) Modelled local (black) current at Goa (B7) and remote contributions from different blocks: B5 (red), B3 (green), and B1 (blue). (e) Observed current off Goa (black) and QuikSCAT winds (ms^{-1}) at each latitude: Tuticorin (red), 8.5°N (green), 10.5°N (blue), and 12.5°N (orange). The amplitude of winds were multiplied by a factor of 3. Note that a positive wind is downwelling-favourable: hence, the Tuticorin wind is positive if the meridional component is equatorward.

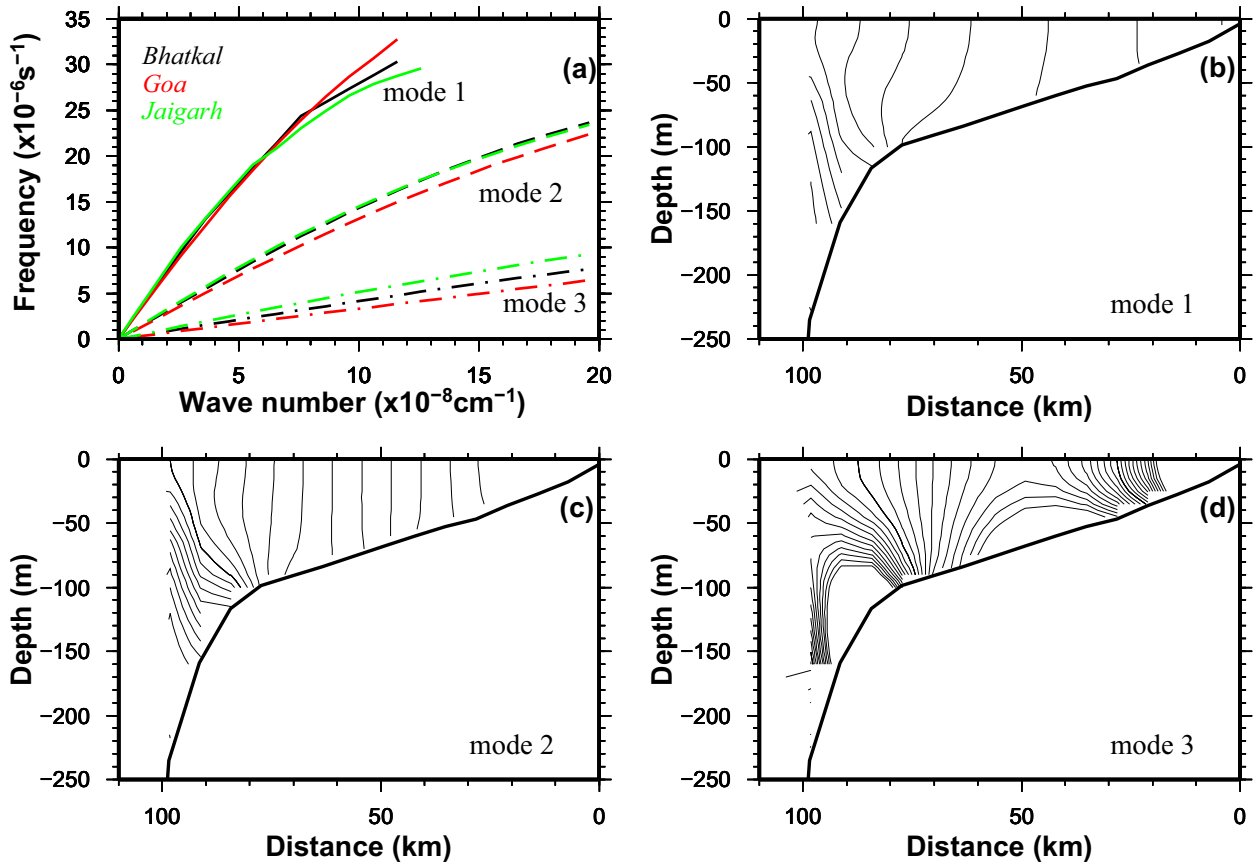


Figure 8: Results of the CTW calculations. (a) Dispersion curve for the first three CTW modes for Bhatkal (black), Goa (red) and Jaigarh (green). (b)–(d) Offshore-vertical structure for the first three modes at Goa; the structure is similar at the other two locations.

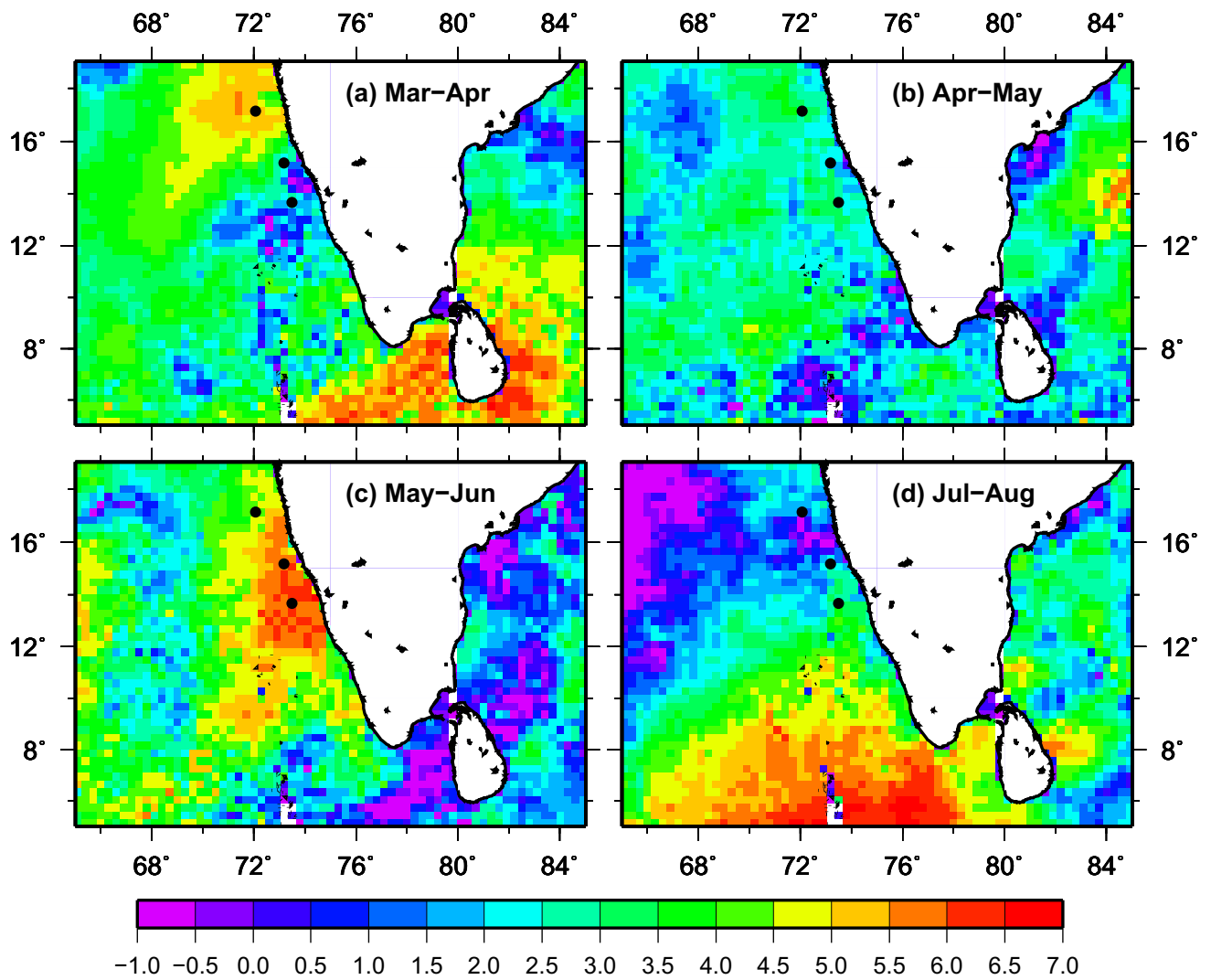


Figure 9: Spatial variation of the wavelet power at the 12-day period for the meridional component of the QuikSCAT winds. In each panel, the wavelet power was averaged over a month. The wavelet power is plotted on a \log_2 scale.

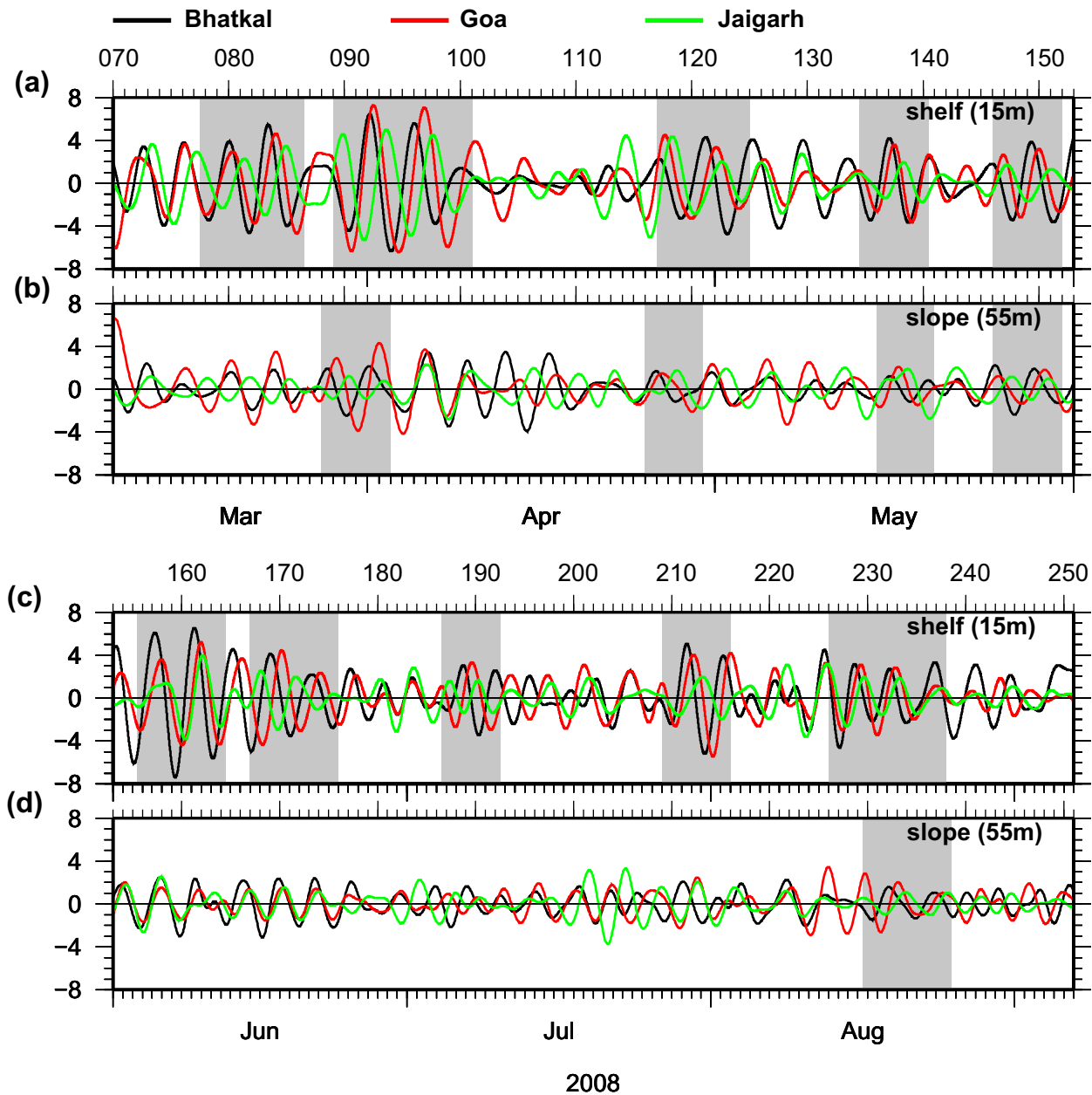


Figure 10: 3–5-day band-passed currents for Bhatkal (black), Goa (red), and Jaigarh (green). The shaded region denotes the period when free wave propagation is observed between the three stations. (a) Shelf current at 15 m during March–May. (b) Slope current at 55 m during March–May (c) Shelf current at 15 m during June–August (d) Slope current at 55 m during June–August.

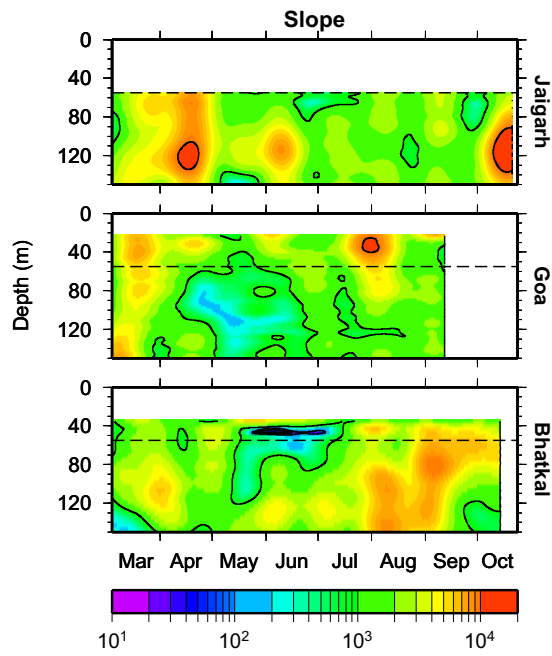


Figure 11: Band-averaged wavelet power spectra of alongshore currents on the slope off Jaigarh (top), Goa (middle), and Bhatkal (bottom) as a function of time and depth for the 12-day period. The dashed line shows the 55 m water column depth on the slope.